Journal of Inorganic Biochemistry 267 (2025) 112875

Contents lists available at ScienceDirect

Journal of Inorganic Biochemistry

journal homepage: www.elsevier.com/locate/jinorgbio

Fluorescent half-salen phenoxy-imine zinc complexes to reveal exogenous and endogenous H_2S

Alessio Trerotola [a], Giuseppe Gravina [a], Viktoriia Vykhovanets [a], Naym Blal [a], Daniela Guarnieri [a], Andrea Maranzana [b], Marina Lamberti [a], Mina Mazzeo [a], Maria Strianese [a,*]

[a] Dipartimento di Chimica e Biologia "Adolfo Zambelli" and INSTM Research Unit, Università degli Studi di Salerno, Via Giovanni Paolo II, 132, 84084 Fisciano, SA, Italy

[b] Dipartimento di Chimica, Università di Torino, via Pietro Giuria 7, I-10125 Torino, TO, Italy

ARTICLE INFO

Keywords:
Fluorescence
Half-salen Zn complexes
H_2S
Sensors
Imaging experiments
DFT calculations

ABSTRACT

In this contribution, the synthesis and the reactivity with HS^- of a family of half-salen Zn complexes are reported. We provide evidence that HS^- binds the zinc center of all the complexes under investigation. DFT and CCSD(T) calculations were performed to model the reactivity of these complexes with HS^-.

We successfully applied a homoleptic zinc complex bearing a Schiff-based ligand with pyridine pendant arms as a probe for the monitoring of exogenous and endogenous H_2S levels in live cells.

1. Introduction

For hundred of years H_2S has been solely known as a toxic gas, causing life destructions and extinctions on the earth. The revolutionary discovery that this molecule is endogenously produced in mammalian tissues and exherts physiological and/or pathophysiological functions within human body, depending on its concentration [1,2], motivates its entrance in the family of the 'so-called' *gasotransmitters* (together with NO and CO) [3,4]. Along with this discovery, better molecular understandings of possible pathways for endogenous H_2S generation and sulfur metabolism began to emerge. By now it is well acknowledged that both enzymatic and nonenzymatic routes contribute to endogenous H_2S generation, and also de-regulation of endogenous H_2S levels has been observed in different diseases such as asthma, Alzheimer, cancer, and other pathological conditions [5,6].

In this context an upsurge of model systems and investigative tools of how H_2S and related Reactive Sulfur Species (RSS) participate in complex biological processes were devised. In particular, fluorescent probes for H_2S detection have been proven as important tools for investigating the composite roles of this molecule in complex biological systems. A new common approach aiming at developing such tools makes use of "activity-based probes" which pair a H_2S-mediated chemical reaction to a fluorescence response [7].

In the last years, we & others focused on metal-based H_2S sensing molecules which exploit the coordination of H_2S, or more commonly HS^-, to transition metal centers (both included in cofactors of natural metalloproteins and as cores of low-molecular weight complexes) [8–23]. This approach offers the additional potential advantage of implementing reversible probes for H_2S detection which harness the reversible coordination of H_2S/HS^- to the metal center.

In the first instance, we focused on square planar salen-based zinc complexes and showed that the electronic state of the diamine moiety between the zinc-chelating nitrogens and/or the substituents on the phenoxide units strongly modulate the photophysical properties of the salen complexes so as their fluorescence response to hydrogen sulfide. Among other factors, we investigated also how the 'hardness/softness' of imine and amine nitrogens which chelate the zinc centers may affect the HS^- binding of the resulting complexes [24]. Since Zn (II) ions have d^{10} configuration with complete outermost orbitals, related complexes do not have crystal field stabilization energy and may adopt different geometries, varying from tetrahedral to octahedral, depending on the hapticity and steric properties of ancillary ligands [25]. In salen-based zinc (II) complexes, because of the structural rigidity generated by the diimine backbone, the Zn(II) is forced in a distorted planar geometry that influences the Lewis acidic character of the zinc atom [26–29]. Differently, zinc complexes of bidentate NO Schiff base ligands, were always found in a pseudo-tetrahedral coordination around the metal centre [30–33].

* Corresponding author.
E-mail address: mstriane@unisa.it (M. Strianese).

https://doi.org/10.1016/j.jinorgbio.2025.112875
Received 12 December 2024; Received in revised form 16 February 2025; Accepted 26 February 2025
Available online 1 March 2025
0162-0134/© 2025 The Authors. Published by Elsevier Inc. This is an open access article under the CC BY license (http://creativecommons.org/licenses/by/4.0/).

In the current work, we selected a family of half-salen phenoxy-imine zinc complexes with the aim to explore whether Zn(II) complexes with more flexible coordinative environments and a tetrahedral coordination geometry could tune the electronic properties and the Lewis acidity of the metal center, thus affecting the propensity of the metal itself to coordinate H_2S/HS^-. A further idea was to investigate whether switching to the half-salen ligands could influence the fluorescence properties of the related species. The final aim is to explore the possible application of bis phenoxy-imine zinc complexes as HS^- sensing molecules in living cells.

To our knowledge, only a single example of zinc complex with a 'half-salen' ligand was previously reported in the literature for H_2S detection and in this case the recognition properties toward H_2S were assayed by UV–vis spectroscopy and for in vitro investigations. For these systems authors propose the H_2S-mediated-Zn displacement as the active recognition mechanism [34]. Another example of half-salen complexes for sensing applications was reported in ref. [35].

The family of complexes under investigation in the present contribution is displayed in Scheme 1. These are simple bis phenoxy-imine Zn (II) complexes (complexes **1** and **2**) in which different substituents have been introduced on the phenoxy fragment.

In addition, complex **3**, in which a pyridine pendant arm was added as new structural element on the ligand skeleton, was selected with the aim to explore if the additional pyridine moiety may offer a contribution to the coordination of the target molecule.

Indeed, previous studies performed in our group, demonstrated that although in the solid-state complex **3** shows a four-coordinated zinc center in a distorted tetrahedral geometry in which the pyridine nitrogen atoms are not involved in the coordination at the metal centre, these additional donors have a crucial role in catalysis [36–39].

2. Experimental section

2.1. Materials

All chemicals used for the synthetic work were obtained from Sigma-Aldrich or Strem Chemicals and were of reagent grade. They were used without further purification. Synthesis of complexes and proligands were performed by following literature procedures [36–39].

2.1.1. General

HR MALDI mass spectra were recorded using a Bruker solariX XR Fourier transform ion cyclotron resonance (FT-ICR) mass spectrometer (Bruker Daltonik GmbH, Bremen, Germany) equipped with a 7 T refrigerated actively-shielded superconducting magnet (Bruker Biospin, Wissembourg, France). The samples were ionized in positive or negative ion mode using the MALDI ion source. The mass range was set to *m/z* 150–2000. The laser power was 15 % and 15 laser shots were used for each scan. Mass spectra were calibrated externally using a mix of peptide clusters in MALDI ionization positive ion mode. A linear calibration was applied. NMR spectra were recorded on a Bruker AVANCE 400 NMR instrument (^{1}H NMR, 400.13 MHz; ^{13}C NMR, 100.62 MHz) or on a 600 MHz spectrometer [600 (^{1}H NMR) and 150 MHz (^{13}C NMR)] using 5 mm o.d. NMR tubes. The chemical shifts were reported in δ (ppm) referenced to SiMe4. Typically, 5 mg of the complex in 0.5 milliliter of the solvent were used for each experiment.

2.2. Syntheses

2.2.1. Synthesis and characterization of complex **1** (bis(2-methoxy)-6-((propilimino)methyl)phenoxy)zinc)

To a stirred solution containing the ligand (2-methoxy)-6-((propilimino)methyl)phenoxy) (0.366 g, 1.89 mmol) in dry Benzene (2.0 milliliter) was added dropwise a solution of $ZnEt_2$ (0.117 g, 0.947 mmol) in dry Benzene (4.0 milliliter), then the solution was stirred overnight at room temperature. The solvent was removed under vacuum, forming a yellow solid. The formation of the desired species was confirmed by NMR analysis. Yield: 95 %.

^{1}H NMR (400 MHz, DMSO-d_6, 298 K): 8.47 (s, 1H, H_d), 6.9 (m, 2H, $H_{e,g}$), 6.49 (dd, $J = 7.8$ Hz, 1H, H_f), 3.69 (s, 3H, OCH_3), 3.51 (t, $J = 7.2$ Hz, 2H, H_c), 1.53 (m, 2H, H_b), 0.81 (t, $J = 7.4$, 3H, H_a). ^{13}C NMR (75 MHz, DMSO-d_6, 298 K): δ 172.4, 161.7, 152.4, 128.7, 117.9, 115.8, 113.2, 62.1, 56.1, 23.7, 11.5.

Emission (DMSO, $\lambda_{exc} = 380$ nm), λ_{max}, nm (quantum yield,Φ_F): 480 nm (0.2).

2.2.2. Synthesis and characterization of complex **2** (bis(3-hydroxy)-6-((propilimino)methyl)phenoxy)zinc)

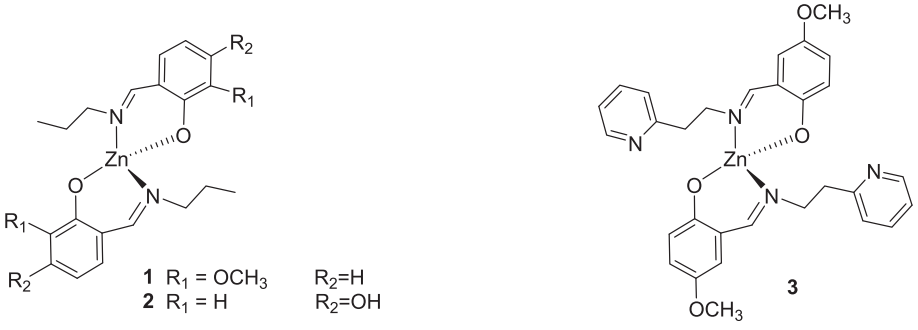
To a stirred solution containing the ligand (3-hydroxy)-6-((propilimino)methyl)phenoxy) (0.538 g, 3.00 mmol) in dry CH_2Cl_2 (8.0 milliliter) was added dropwise a solution of $ZnEt_2$ (0.204 g, 1.65 mmol) in dry CH_2Cl_2(4.0 milliliter), then the solution was stirred overnight at room temperature. The solvent was removed under vacuum, forming a dark-white solid. The formation of the desired species was confirmed by NMR analysis. Yield: 95 %.

^{1}H NMR (400 MHz, DMSO-d_6, 298 K): 8.24 (s, 1H, H_d), 7.05 (d, $J = 8.5$ Hz, 1H, H_E), 6.06 (dd, $J_1 = 8.5$ Hz $J_2 = 2.0$ Hz1H, H_f), 5.99 (d, $J = 2.0$ Hz, 1H, H_g), 3.40 (t, $J = 7.1$ Hz, 2H, H_c), 1.49 (m, 2H, H_b), 0.80 (t, $J = 7.2$, 3H, H_a). ^{13}C NMR (75 MHz, DMSO-d_6, 298 K): δ 172.3, 170.5, 163.8, 138.0, 112.2, 106.5, 104.9, 61.6, 23.6, 11.4.

Emission (DMSO, $\lambda_{exc} = 352$ nm), λ_{max}, nm (quantum yield,Φ_F): 420 nm (0.5).

2.2.3. Synthesis and characterization of complex **3** ((bis(4-methoxy)-2-(((2-(pyridin-2-yl)-ethyl)imino)methyl)phenoxy)zinc)

Into the glove box, in a 20 milliliter vial are put 0.501 g (1.95 mmol, 2 eq.) of the ligand (4-methoxy)-2-(((2-(pyridin-2-yl)-ethyl)imino) methyl)phenoxy were weighted and dissolved in 3 milliliter of benzene, then 0.98 milliliter (0.98 mmol) of $ZnEt_2$ 1 M benzene solution was diluted in 5 milliliter of dry benzene. The $ZnEt_2$ solution was added drop by drop with a syringe. The reaction medium was agitated with a magnetic stirring for 6 h. At the end of the reaction, the benzene was



Scheme 1. Structures of the complexes investigated in this work

removed under vacuum. The resulting solid was washed with dry hexane. Yield 78.2 %.

^{1}H NMR (400 MHz, DMSO-d_6, 298 K): 8.45 (2H, d, J = 4.4 Hz, –CH ortho-pyridine), 8.33 (2H, s, HC═N), 7.66 (2H, t, J = 7.7 Hz, Ar), 7.19 (2H, m, Ar), 6.93 (2H, m, Ar), 6.74 (2H, d, J = 3.3 Hz Ar), 6.63 (2H, d, J = 9.0 Hz, Ar), 3.90 (4H, t, J = 7.4 Hz, N–CH_2–CH_2–C), 3.65 (6H, s,–O–CH_3), 3.03 (4H, t, J = 6.9 Hz, N–CH_2–CH_2–C). ^{13}C NMR (75 MHz, C_6D_6, 298 K): δ 171.4, 163.4, 158.6, 153.2, 149.0, 135.8, 124.3, 120.9, 118.9, 116.3, 112.7, 60.1, 55.9, 38.0.

Emission (DMSO, λ_{exc} = 400 nm), λ_{max}, nm (quantum yield,Φ_F): 505 nm (0.16).

2.3. Absorbance and fluorescence measurements

Absorption spectra were recorded on a Cary-50 Spectrophotometer, using a 1 cm quartz cuvette (Hellma Benelux bv, Rijswijk, Netherlands) and a slit-width equivalent to a bandwidth of 5 nm. Fluorescence spectra were measured on a Cary Eclipse Spectrophotometer in a 10 × 10 mm^2 airtight quartz fluorescence cuvette (Hellma Benelux bv, Rijswijk, Netherlands) with an emission band-pass of 10 nm and an excitation band-pass of 5 nm. Both absorption and fluorescence measurements were performed either in DMSO or in Milliq water solutions at 25 °C. Fluorescence emission spectra were registered by exciting the samples at a specific wavelength (as stated in the figure captions).

Fluorescence quantum yield (Φ_F) values were measured in optically diluted solutions using as standard the commercial dye Cy3 NHS (Φ_F = 0.15 in MilliQ water), according to the equation: [40].

$$\Phi_F{}^s = \Phi_F{}^r\,(I_s/I_r)(A_r/A_s)(\eta_s/\eta_r)^2$$

where indexes s and r denote the sample and reference, respectively. I stands for the integrated emission intensity, A is the absorbance at the excitation wavelength, and η is the refractive index of the solvent. The optical density of complexesand standards was kept below 0.1. The uncertainty in the determination of $\Phi_F$is ± 15 %.

2.4. Calculation of the limit of detection (LOD)

In agreement with the IUPAC recommendation [41,42], the limit of detection for complex **1** for HS^- was calculated from the spectrofluorometric titration data, using the following equation:

$$LOD = 3\,s/K$$

where s and K represent, respectively, the standard deviation of the blank and the absolute value of the slope of the calibration line (Fig. S19). All data involved in the calculation of LOD are reported in Table S1.

2.5. NMR characterization of the complexes *1*–*3* upon addition of HS^-

The NMR tube was charged with the free complex solutions in DMSO-d_6 then NaSH solid or in solution (to the end concentrations specified in the figure captions) was added and the spectra registered.

2.6. Fluorescence in HBSS

Before fluorescence imaging experiments we studied probe potential in solvents and concentrations close to biological conditions as HBSS. We prepared a 1 mg/milliliter probe solution dissolving complex **3** in DMSO, then we diluted the stock solution in HBSS to have increasing concentrations of the probe. We added 100 μl for each well in a 96-multiwell plate for each sample. Only for probe-HS^- samples we added 50 μl of 3 mg/ml [NaHS]. After that, we analyzed fluorescence intensities with SpectraMax Mini Multi-Mode Microplate Reader (Molecular Device).

2.7. Cell culture

HepG2 cells (Human hepatocellular liver carcinoma cell line) were grown in Minimum Essential Medium (MEM) supplemented with 10 % fetal bovine serum (FBS), 2 mM Glutamine, 1 mM non-essential amino acids and 1 % antibiotics (penicillin/streptomycin, 100 U/milliliter). Cells were maintained in a humidified incubator at 37 °C, in 5 % CO_2/95 % air. 1,5 × 10^5 cells/well were seeded on 12-well multiwell plates one day before imaging.

2.8. MTT assay

Cell viability was analyzed by 3-(4,5-dimethylthiazol-2-yl)-2,5-diphenyltetrazolium bromide (MTT; Sigma-Aldrich) assay. Then, 1.5 × 10^4 cells were seeded in each well of a 96-multiwell plate. Twenty-four hours after cell seeding, HepG2 cells were incubated with increasing concentrations of complex **3** (0.05, 0.5, 5, and 50 μg/ milliliter) obtained by diluting complex **3** stock solution (1 mg/milliliter in DMSO) in cell culture medium. After 2 h of incubation with complex **3** solutions, the MTT reagent was added to the cell media of each sample (final concentration 0.125 mg/milliliter) and incubated for 1 h at 37 °C. The resulting formazan crystals were dissolved in DMSO. Absorbance was measured at 570 and 690 nm wavelengths by a multiplate reader, and raw data were normalized to non-treated cells (considered 100 %) to calculate cell viability percentage. Data were reported as mean ± standard deviation (n = 8).

2.9. Fluorescence imaging

To verify the loading of the probe and capability in H_2S detection, HepG2 cells were incubated with 90 μM complex **3** diluted in cell culture medium for 2 h at 37 °C. After incubation, cells were rinsed to remove excess of complex. Probe-loaded cells were observed by an automated inverted fluorescence microscope (Olympus IX83) at 362–388 nm excitation wavelength and a 10× objective. Only probe-loaded cells were further treated with exogenous NaSH (260 μM in MEM) for 10 min and then observed with the microscope to test the capability of complex to monitor the intracellular increase of H_2S.

To verify capability of complex to monitor endogenous H_2S HepG2 cells were incubated with 90 μM complex diluted in MEM for 2 h at 37 °C. After incubation, cells were rinsed to remove excess of complex and irradiated with UV-C lamp (Spectroline ENF240C) at distance of 50 cm to achieve 40 J/m^2 (~3 s exposure). After exposure the cells were grown in the same medium as before UV irradiation for 3 h. Cells were observed by an epifluorescence microscope (Olympus) at 362–388 nm excitation wavelength and a 10× objective. Similar procedures were applied for the cysteine (1 mM) and H_2O_2 (800 μM) experiments [43,44].

To have a quantitative evidence of the fluorescence enhancement we analyzed the fluorescence intensity/area through ImageJ software. We set five fixed areas and measured the fluorescence intensity for each sample.

2.10. Computational methods

The DFT M06 functional [45] and the def2-TZVP basis set [46,47] were used in conjunction with gradient procedures to determine the minimum and transition structures of chemical interest on the ground state energy hypersurface. The nature of the critical points (and thermochemistry) was assessed using vibrational analysis.

Thermochemical corrections were used to estimate the relative Gibbs free energies (ΔG). The ΔG values, in kcal mol^{-1}, at T = 298.15 K, are reported in the paper.

The reacting systems were examined as a solute within a polarized continuum, which was immersed in DMSO as a solvent. This was accomplished through the use of the Solvation Model based on Density

(SMD) [48] and Integral Equation Formalism-Polarizable Continuum Model (IEF-PCM) schemes in the PCM framework [49].

S_1 states were optimized at the same computational level. Emission spectra were simulated by using single point TD-DFT with O3LYP functional [50].

Vibrational frequencies were scaled by factor 0.982. Quasi-harmonic treatment proposed by Grimme [51] for frequencies below 100 cm^{-1} was applied. Thermochemical corrections were carried out by the program Goodvibes [52].

The energies were then refined by single-point DLPNO-CCSD(T) [53] energy computations with Dunning's cc-pV*TZ* basis set [53,54], including the solvent (DMSO) effect by CPCM [55]. Coupled cluster calculations were performed using ORCA software [56], version 5.0.4.

Geometry optimizations and thermochemical calculations were performed using the GAUSSIAN16 program [57]. Figures have been obtained by the program MOLDEN [58] and Gaussview [59].

3. Results and discussions

3.1. Synthesis and characterization of the complexes

Ligands were prepared by Schiff-base condensation, as reported in the literature [36]. Complexes **1**–**3** were synthesized by reacting the ligands with diethylzinc in benzene, by literature procedures [36–39]. Ligands and complexes were characterized by ^{1}H NMR spectroscopy and high-resolution MS (Figs. S1-S9).

The ^{1}H NMR spectra of complexes **1–3** revealed symmetric structures in solution for all complexes, coherently with the crystal structures observed in the solid state by RX analysis that feature four-coordinated zinc centers in a distorted tetrahedral geometry [37]. The same coordination geometry was observed for complex **3** with the pyridine pendant arms rotated away from the metal centre and not involved in the coordination.

3.2. ^{1}H NMR spectral study

After characterization of complexes **1–3,** we explored whether they were able to form stable adducts with HS^- via ^{1}H NMR spectroscopy.

Fig. 1 displays the ^{1}H NMR spectrum of complex **1** after addition of 1 equivalent of NaSH.

In the spectrum, the presence of two signals at −2.23 and − 2.48 ppm which, according to the literature, are attributable to the protons of HS^- bound to the zinc ion [10,16,23,49,60,61] and, correspondingly, the evidence of two singlets (at 8.16 and 8.56 ppm, respectively) for the imine protons, suggests the existence of the two adducts in 0.4: 1 ratio. Both species are highly symmetric, showing a single set of signals for the protons of two equivalent ligands. We performed additional experiments varying the acquisition temperature between 25 °C and 95 °C: the resulting ^{1}H NMR spectra are displayed in Fig. S10. At high temperatures both the protonic patterns of the two adducts are still distinguishable.

The coordination of SH^- to zinc complexes **1–3**, would result in a penta-coordinate geometry around Zn. For penta-coordinate Zn complexes, both square pyramidal (SP) [62–65] and trigonal bi-pyramidal (TBP) [66–70] geometries are common. Penta-coordinate metal complexes are known to be stereochemically non-rigid species, and molecules with trigonal bi-pyramidal geometry are known to isomerize by the Berry pseudo-rotation mechanism [71,72].

Differently than complex **1**, the addition of NaSH to a DMSO-d_6 solution of complex **2** results in the formation of a single symmetrical adduct (see Figs. S11 and S24): the resonances of the two salicylaldiminato units appeared as equivalent. Again, the high field signal at −2.3 ppm of the HS^-zinc coordinated group is clearly evident and integrates for 1 proton with respect to the presence of two phenoxy-imino ligands coordinated to the zinc center.

Analogously, for complex **3**, the addition of 1 equivalent of NaSH to the DMSO-d_6 solution of the starting complex results in the formation of a single symmetrical adduct (see Scheme 2 and Fig. 2).

As said above, pentacoordinate metal complexes can adopt two different geometries namely TBP and SP. Factors influencing the geometry are the steric encumbrance and the electronic characteristics of the ligands [73,74]. In view of the close stability of SP and TBP forms for penta-coordinated complexes of d^{10} metals such as Zn (II), intramolecular rearrangement might be expected to occur readily.

3.3. Density functional theory study

To gain better insight into the structures of the complexes under investigation and of their different adducts with HS^-, we performed a computational analysis using density functional theory (DFT) and coupled-cluster theory with single, double and perturbative triple excitations CCSD(T) methods.

In our cases, all complexes preferred a mixed TBP and SP geometry. All attempts to optimize the perfect square-pyramidal trigonal

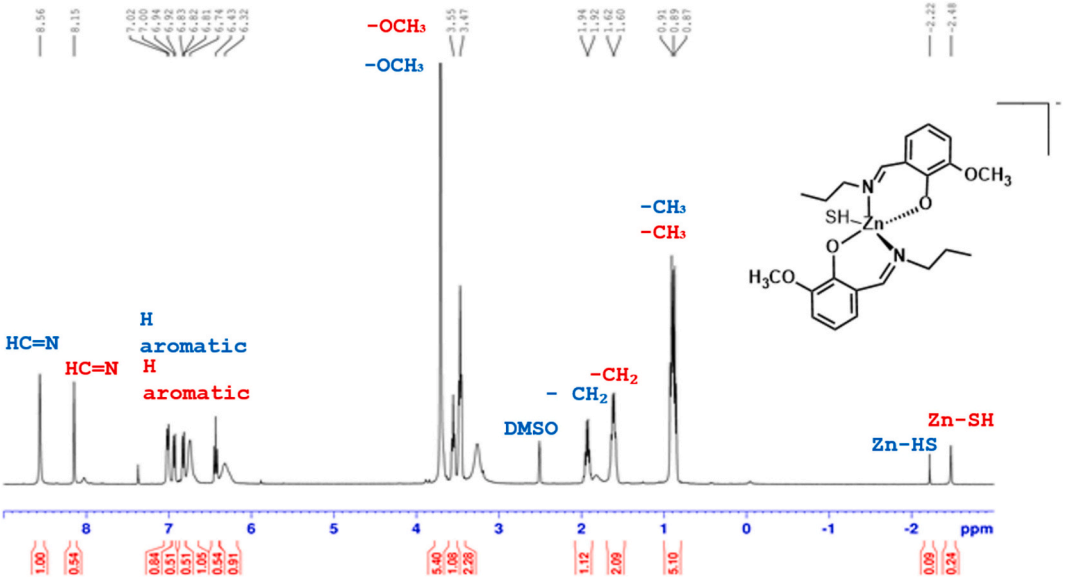
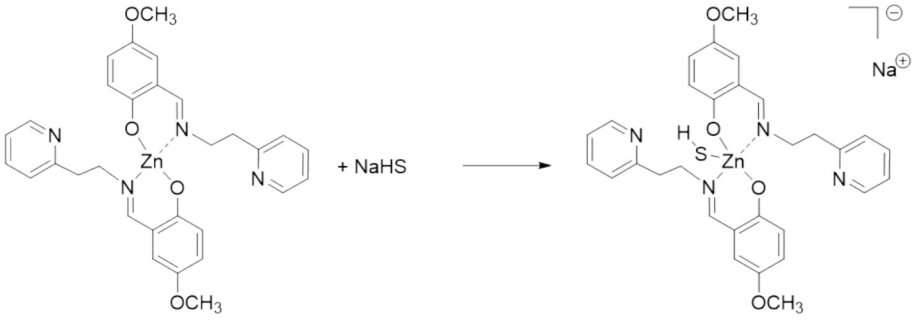


Fig. 1. ^{1}H NMR spectrum of complex **1** in DMSO-d_6 after the addition of HS^-. [complex **1**] = [NaSH] = 5*10^{-2} M. (400 MHz, DMSO-d_6, 298 K).



Scheme 2. Schematic reaction of complex **3** with NaSH and formation of the related HS-adduct (DMSO-d_6, 20 °C).

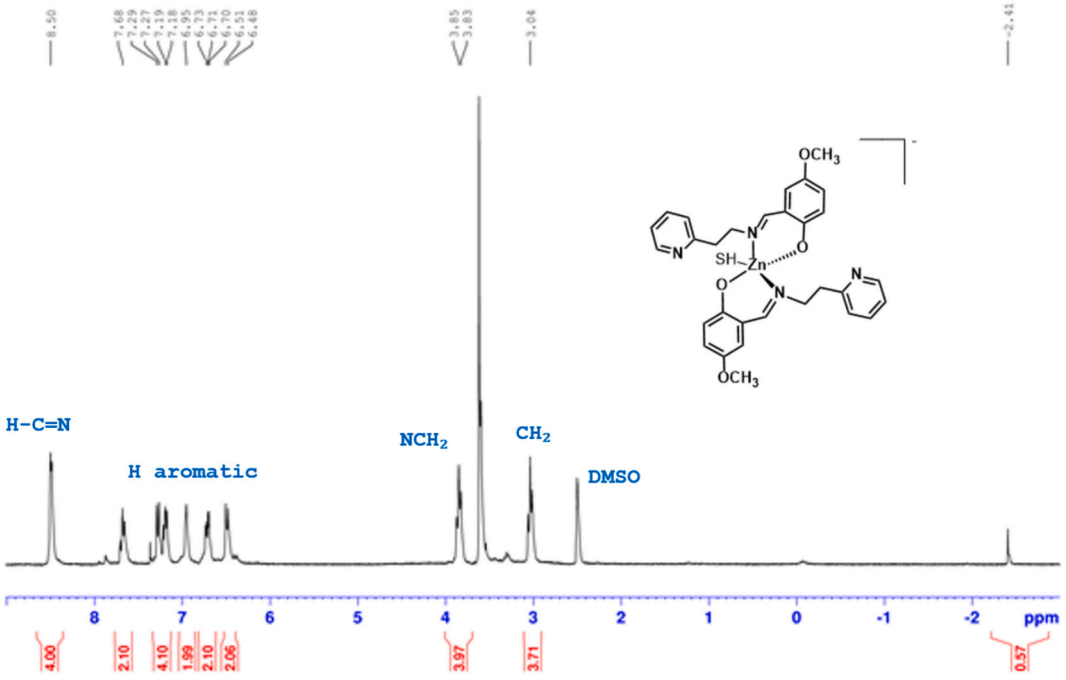


Fig. 2. ^{1}H NMR spectrum of complex **3** in DMSO-d_6 after the addition of HS^-. [complex **3**] = [NaSH] = 5*10^{-2} M. (600 MHz, DMSO-d_6, 298 K).

bipyramid failed. The index of the degree of trigonality (τ) of the five-coordinate structures was reported: for a perfectly square pyramidal geometry, τ is equal to 0, while it becomes 1 for a perfectly trigonal-bipyramidal geometry [75].

Three types of trigonal-bipyramidal-like structures were found for each of the four complexes (τ ranging from 0.63 to 0.81, in Table 1): NN axial, OO axial and NO axial, as shown in Fig. 3. The first two structures lead to symmetrical complexes (pseudo C2 symmetry), whereas the SH-complex with N and O ligands in axial positions is asymmetrical (C1 symmetry).

In complexes **1–3**, OO axial geometries were the most stable. The stabilities of the NO and NN geometries depend on the substituents. The calculated relative free energies are presented in Table 1. NN axial complexes are, in general, the least stable intermediate: 1.8–3.6 kcal mol^{-1} less stable than the OO axial complexes.

Complexes **2** and **3** show a single peak in the ^{1}H NMR spectrum for the imine protons, consistent with the relative stability of the OO axial isomer, which has C2 symmetry; therefore, the two ligands are equivalent. According to their relative energies, the other isomers (NO and NN axial) are present in negligible amounts compared to the OO axial isomer.

On the other hand, for complex **1**, the OO axial intermediate is dominant, but the NN axial isomer is not negligible: it lays only 0.6–0.3 kcal mol^{-1} above the OO axial intermediate. In terms of equilibrium constants, the $[OO_{axial}]/[NN_{axial}]$ ratio is about 1.7–2.8, depending on the level of calculation. Similar values for the relative free energies at high temperature were calculated. Qualitatively these numbers are consistent with the ratio between the two symmetric structures observed in the ^{1}H NMR spectra (Fig. 1 and Fig. S20).

Table 1
Degree of trigonality (τ) and relative free energies in kcal mol^{-1}, at 298 K, calculated at M06/def2-TZVT and DLPNO-CCSD(T)/cc-pVTZ//DFT level.

	complex **1**			complex **2**			complex **3**		
	M06	CCSD(T)	τ	M06	CCSD(T)	τ	M06	CCSD(T)	τ
NN_{axial}	0.56	0.25	0.74	1.79	2.28	0.69	2.14	3.64	0.71
NO_{axial}	2.27	1.49	0.81	1.49	1.53	0.75	2.08	2.36	0.77
OO_{axial}	0.00	0.00	0.76	0.00	0.00	0.78	0.00	0.00	0.73

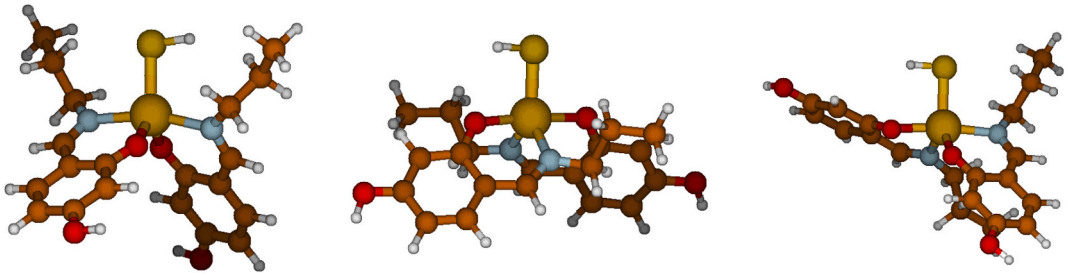


Fig. 3. Complex **2** NN axial (left), OO axial (center), and NO axial (right).

3.4. Optical study

In a second instance, we investigated the optical properties of complexes **1**–**3** in the presence of NaSH.

Fig. 4 displays the electronic absorption spectra of the complexes.

All the complexes under investigation show absorption bands in the UV region (ca. 300–400 nm). In the presence of HS^- visible changes of the initial absorption spectra of all the complexes occurred, thus confirming the formation of new species. In the case of complexes **1** and **3** the Uv-vis spectra do not exhibit significant shifts but an enhancement of the absorption maxima was observed. Differently complex **2**, in the presence of HS^-, undergoes an evident bathochromic shift as reported in the literature for other zinc complexes upon coordination of an analyte [76,77].

Next, we studied the fluorescence response of complexes **1**–**3** before and after HS^- addition, the outcome of these experiments is displayed in Fig. 5.

The addition of an equal amount of HS^- to the complexes **1**–**3** leads to different degrees of fluorescence switching as shown in Fig. 5. The quenching efficiency or switching ratio (SR) (%) (%) is evaluated by the eq. $(F - F_0)/F$ x 100, where F_0 and F are the luminescence intensities of complexes before and after the addition of the target analyte, respectively. It was observed that the analyte decreases the emission intensity of the complexes **1** and **2**, and the decreasing order of quenching efficiency is 2 > 1.

Complex **3**, after the addition of HS^- as analyte, undergoes a fluorescence enhancement of 55 %.

The simulated emission spectra with the SH anion (Fig. S12) are in good agreement with the spectra reported in Fig. 5. The O3LYP functional slightly underestimated the λ_{max} by 15–20 nm. The $S_1 \rightarrow S_0$ bands

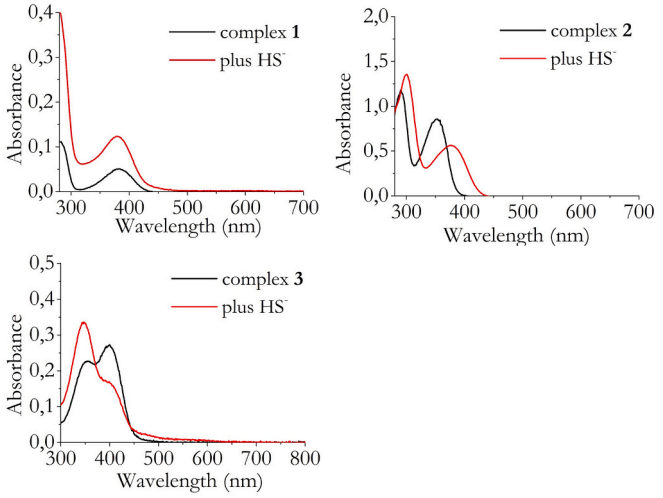


Fig. 4. Electronic absorption spectra of complexes **1**–**3** with and without the addition of 10 μM of NaSH. The spectra were recorded in DMSO with complexes concentration of 10 μM.

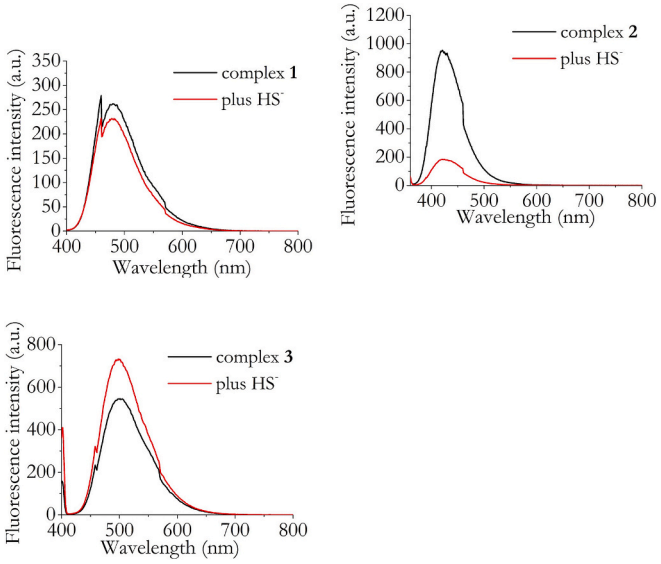


Fig. 5. Emission spectra of complexes **1**–**3** before and after the addition of 1 equiv. of NaSH. [Complexes **1**–**3**] = 1×10^{-5} M; [NaSH] = 1×10^{-5} M. All spectra were registered in DMSO with λ_{exc} = 380 nm for complex **1**; λ_{exc} = 352 nm for complex **2**; λ_{exc} = 400 nm for complex **3**. SRs: complex **1** = 10 %; complex **2** = 80 %; complex **3** = 55 %.

were dominated by the electron transitions π–π* (HOMOs-LUMOs). Four triplet states were found to be close in energy to that of the S1 excited state. For complex **2**-SH, triplet states were formed by electron excitations from orbitals #119 to #120 (T**1**), #118–121 (T_2), #116–120 (T_3), #119–121 (T_4). An image of the relevant molecular orbitals is shown in Figs. S13 and S14.

T_1, T_2, and T_4 correspond to electronic transitions from π to π* orbitals, whereas T_3 is an n–π * transition. Because S_1 and T_3 are close in energy and according to the El-Sayed rule [78], S_1-T_3 intersystemcrossing is supposed to be relatively fast compared to the other S_1-T_x crossing. The decrease in the complex **2**-SH emission could be ascribed to this fast S_1-T_3 intersystem crossing.

For complex **3** with SH, triplet states were formed by electron excitations from orbitals #159–160 (T_1), #158–161 (T_2), #159–161 (T_3), #158–160 (T_4). All these transitions involve π and π* orbitals. We can suppose that the intersystem crossing S_1-T_x is slow, and consequently the emission S_1-S_0 is intense.

Following our screening of the optical features of the complexes under investigation, we explored their potential in living cells. For the experiments we selected complex **3** which seemed the most promising in the preliminary fluorescence experiments in vitro (see Fig. 5).

To obtain an indication on the selectivity of complex **3** for HS^- recognition, its fluorescence intensity in the presence of biologically relevant and potentially competing thiols or in the presence of a range of anions or of common oxidants was checked. Fig. S15 shows the obtained results. For the competitors investigated we observed a quenching of the

initial fluorescence intensity of complex **3** with the only exception of chloride for which a very modest raise of the initial fuorescence was registered. This finding suggests a good selectivity of our probe under the experimental conditions tested.

When monitoring the electronic absorption spectra of complex **3** in the presence of increasing amounts of HS^- a gradual change is registered (Fig. S16 in the SI).

To assess whether also the fluorescence response is dependent on the HS^- concentration, we monitored the change of the initial fluorescence intensity of complex **3** after the addition of increasing concentrations of NaSH. The response of the fluorescence switching of complex **3** for a series of subsequent measurements with increased concentrations of NaSH is reported in Fig. S16. In these experimental conditions a binding affinity constant (K_b) of $2.3*10^4$ was quoted (Fig. S17). When monitoring the fluorescence intensity of complex **3** in the presence of increasing concentrations of NaSH but exciting the complex at the isosbestic point (i.e. 370 nm, see Fig. S16 (a)) we still observed a gradual increase of the fluorescence (Fig. S18).

The limit of detection (LOD) of complex **3** for HS^- was found to be in the sub-micromolar range (Fig. S19 and Table S1 in the SI).

Before starting cell imaging experiments, we checked whether complex **3** gives a fluorescence response in conditions more compatible with cell cultures (e.g. in Milliq water solutions). Fig. S20 displays the absorption and fluorescence responses of complex **3** in these conditions and when increasing the HS^- concentration. Futhermore we also checked whether the fluorescence response of complex **3** is modulated by HS^- when diluting the complex itself in Hank's Balanced Salt Solution (HBSS). The outcome of this experiment is displayed in Fig. S21. Also in these experimental conditions, in the presence of HS^- a fluorescence enhancement was observed at all the concentrations of complex **3** tested.

3.5. Biological study

Next, we assessed the cytotoxicity of our probe via a MTT experiment. The MTT assay in HepG2 cells showed that complex **3** was slightly toxic under the experimental conditions tested (Fig. S22).

Then we investigated the ability of complex **3** to visualize exogenous H_2S in HepG2 cells. Therefore, we first incubated the cells for 2 h with our probe (90 μM) to explore whether the complex was able to permeate the cells. Fig. 6 shows the cells after treatment with the sensing complex. A little fluorescence enhancement is evident thus indicating that the probe entered the cells (Fig. 6B). We then incubated the cells for 10 min with a DMSO solution of HS^- to check if the intracellular formation of the complex **3**/HS^- binding adduct occurs. A visible fluorescence enhancement of the cells was observed (Fig. 6C) thus highlighting the potential of complex **3** to detect HS^- directly inside the cells and its stability in cell culture conditions.

With these results in hands we decided to investigate the ability of complex **3** to visualize endogenous H_2S in HepG2 cells. As reported in the literature, UV-C irradiation of the cells results in the endogenous H_2S release of the cells, as response to the stimulus [79,80]. More specifically, UV irradiation induces the production of Reactive Oxygen Species (ROS) that, in turn, promotes H_2S release in the cells [79]. To this end, we irradiated the cells with a UV-C lamp (Fig. 7B) (Spectroline ENF240C) at a distance of 50 cm to achieve 40 J/m^2 (~3 s exposure). After exposure, the cells were grown in the same medium as before UV irradiation and incubated with complex **3** for 2 h: a light fluorescence enhancement of the cells was immediately observed (Fig. 7C). When monitoring the fluorescence of the cells incubated with complex **3** and exposed to the UV lamp (3 h after the UV irradiation) an evident fluorescence enhancement could be observed (Fig. 7D). The last finding demonstrates capability of complex **3** to detect endogenous H_2S content. Most likely 3 h is the time interval which the cells need to produce an amount of endogenous H_2S detectable by complex **3**.

To gain quantitative evidence of the fluorescence enhancement observed when comparing the fluorescence of the cells incubated with complex **3** with that of the cells incubated with complex **3** and exposed to UV irradiation (after 3 h), we investigated the fluorescence intensity/area through the ImageJ software (Fig. 8). The results clearly evidence a raise in the initial fluorescence intensity of complex **3**.

In a different experiment, after incubating HepG2 cells with complex **3** and exposing them to UV irradiation, we also added a known amount of exogenous H_2S and measured the fluorescence of the cells under the microscope after 15 min from treatments (Fig. 9). In the latter experiment, as clearly evident from Fig. 9D, an immediate raise in the fluorescence of the cells could be detected. Taken altogether these results indicate that the complex **3** is easily absorbed by the cells (already after 2 h of incubation), as evidenced by the experiment reported in Fig. 9, and, most importantly, it is retained by cells allowing the detection of endogenous H_2S (Figs. 7 and 8).

By now it is well acknowledged that genomic lesions produced by various DNA damaging agents (e.g. UV-irradiation, ROS species, mutagenic chemicals) trigger several specific repair machinery to conserve the genomic integrity [81]. In particular harsh conditions that exist in the tumor microenvironment, including hypoxia, glucose deprivation, cysteine and hydrogen peroxide (H_2O_2) incubation of the cells, which all lead to cell damage and acute stress, result in intracellular H_2S release [44]. Thus we explored whether the response of complex **3** in the presence of ROS-stimulated-HepG2 cells would parallel the fluorescence

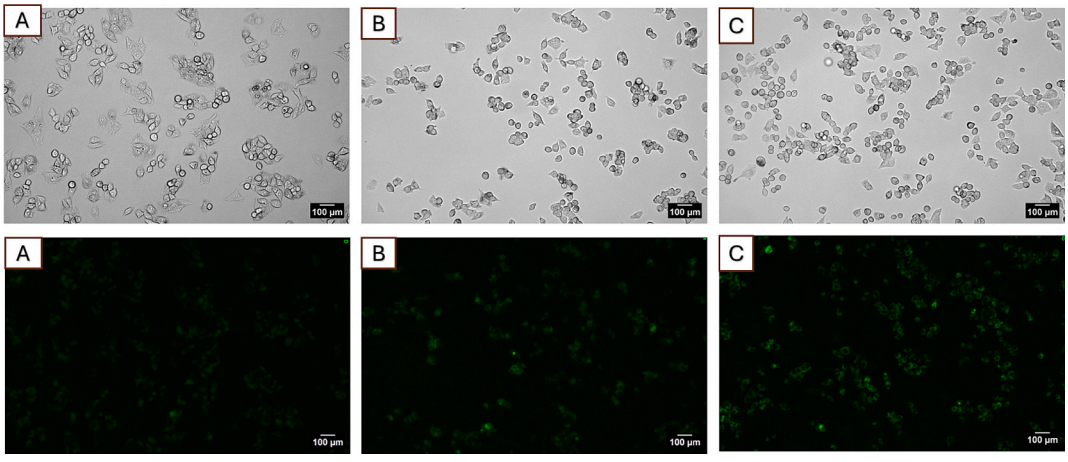


Fig. 6. Fluorescence microscopy images of non-treated HepG2 cells (a) and HepG2 cells after 2 h treatment with 90 μM complex **3** (b) and 90 μM complex **3** + 260 μM NaSH treatment for 10 min (c). Magnification bar 10× objective.

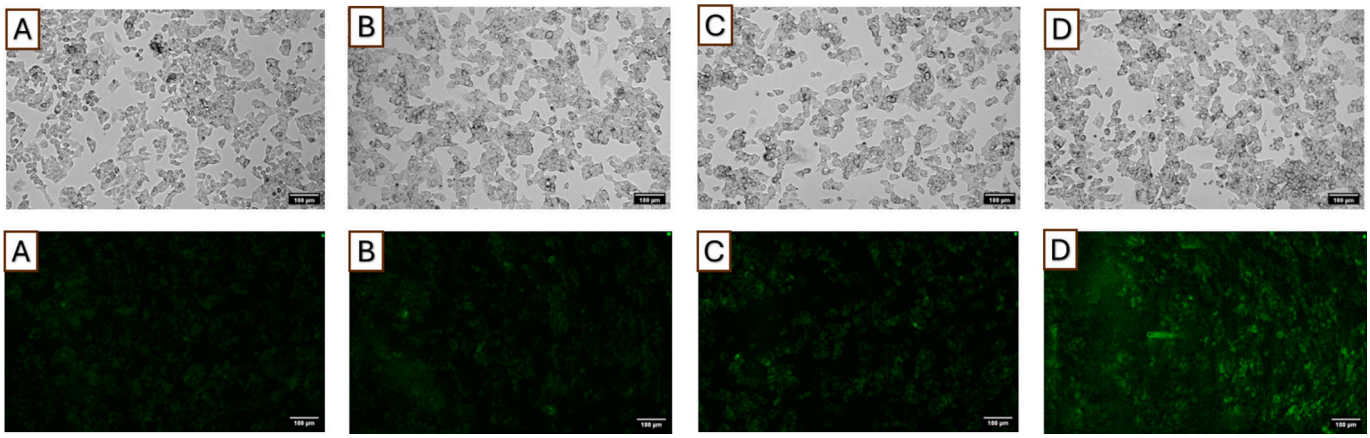


Fig. 7. Fluorescence microscopy images of non-treated HepG2 cells (A), HepG2 cells 3 h after UV-C irradiation (~3 s, 40 J/m^2) (B), HepG2 cells 2 h after the treatment with 90 μM complex (C) HepG2 cells treated with 90 μM complex + UV-C irradiation (~3 s, 40 J/m^2) 3 h after the treatment (D).

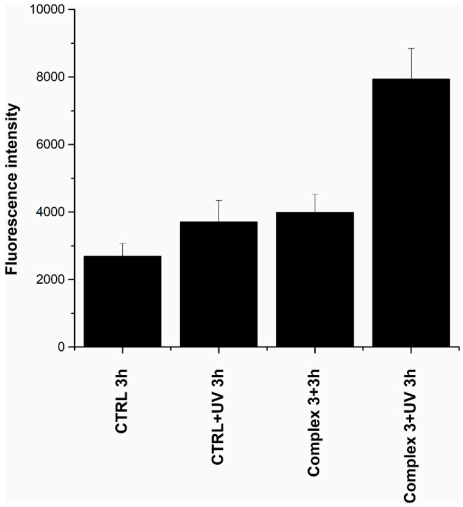


Fig. 8. Quantification of fluorescence intensity/area 3 h after UV irradiation in the presence of complex **3** (Complex **3** + UV 3 h) and absence of complex **3** (CTRL+UV 3 h) compared to non-treated cells, used as control (CTRL 3 h) and cells treated only with complex **3** (Complex **3** 3 h).

response observed upon UV irradiation.

More specifically, after incubation of the cells with complex **3** we feeded the cells with either cysteine [43] or H_2O_2 [44] following literature conditions and monitored their fluorescence. As visible in Fig. 10D and Fig. S23D a fluorescence enhancement was observed in both cases.

4. Conclusions

In this work we provide evidence that homoleptic zinc complexes bearing *half-salen* ligands can successfully function as H_2S revealing molecules by a coordinative-based approach: all the studied complexes are able to coordinate HS^- forming the corresponding adduct(s). While in the case of complex **1** the reaction gave two different isomers, for complexes **2** and **3** the selective formation of a single adduct was observed. DFT and CCSD(T) calculations were performed to model the reactivity of these complexes with HS^-. The optimized structures of the NN, NO, and OO axial complexes and their relative energies are consistent with the ^{1}H NMR spectra of the HS-treated complexes. Fluorescence spectra showed a turn-on response for complex **3** in the presence of HS^- and a marked selectivity in the presence of possible competitors, suggesting that it is the most suitable of the title complexes for HS^- sensing. Biological experiments further confirm the ability of complex **3** to detect H_2S in the intracellular environment making it a promising candidate for the development of effective strategies in biomedical applications. To our knowledge it constitutes one of the first examples of complexes with a bidentate-salen ligand used for this

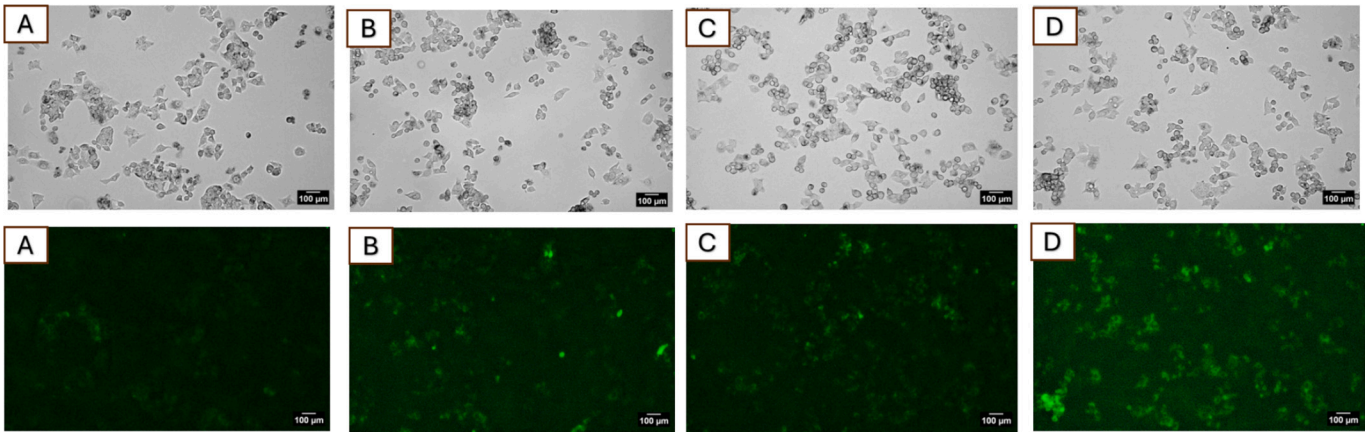


Fig. 9. Fluorescence microscopy images of non-treated HepG2 cells (A), HepG2 cells after 2 h treatment with 90 μM complex (B), 90 μM complex + UV-C irradiation (~3 s, 40 J/m^2) after 15 min from treatment (C) and 90 μM complex + UV-C irradiation (~3 s, 40 J/m^2) + 260 μM NaSH (exogenous HS^-) after 10 min from treatment (D).

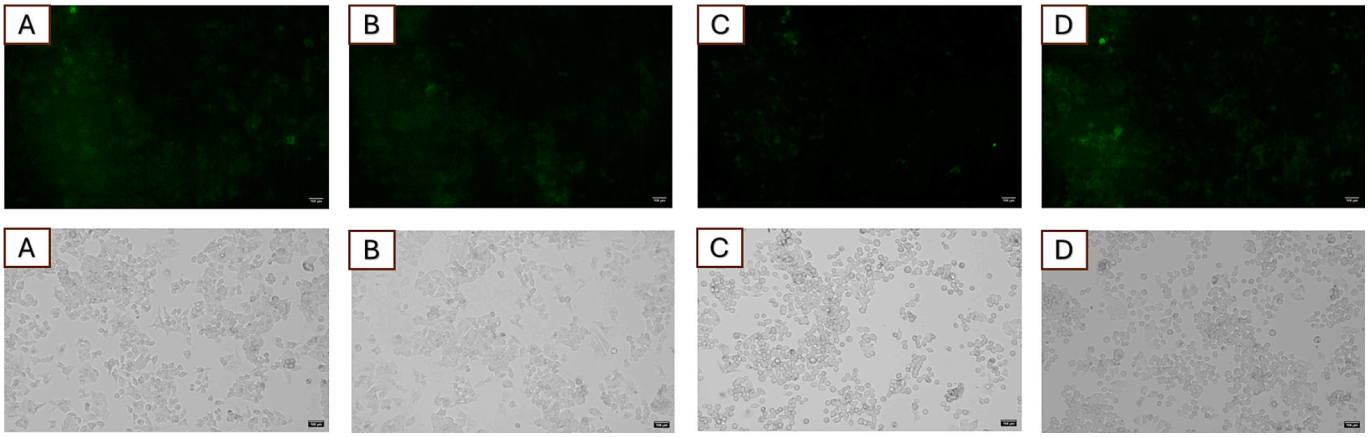


Fig. 10. Fluorescence microscopy images of non-treated HepG2 cells (A), HepG2 cells + cysteine after 30 min from treatment (B), HepG2 cells after 2 h treatment with 90 μM complex (C) and HepG2 cells after 2 h treatment with 90 μM complex + cysteine (1 mM) after 30 min from incubation (D).

purpose.

CRediT authorship contribution statement

Alessio Trerotola: Methodology, Investigation. **Giuseppe Gravina:** Investigation. **Viktoriia Vykhovanets:** Investigation. **Naym Blal:** Investigation. **Daniela Guarnieri:** Data curation. **Andrea Maranzana:** Investigation, Data curation. **Marina Lamberti:** Methodology, Data curation. **Mina Mazzeo:** Writing – review & editing, Methodology. **Maria Strianese:** Writing – review & editing, Writing – original draft, Investigation, Formal analysis, Conceptualization.

Declaration of competing interest

Authors declare no conflict of interest.

Acknowledgments

The computational study was founded by "Finanziato dall''Unione Europea- Next Generation EU, Missione 4 Componente 1 CUP D13C22001340001 - CN00000013", Spoke 7- Materials and Molecular Sciences, Università di Torino. Authors also thank Professor Francesco De Riccardis of 'Università degli Studi di Salerno' for useful discussions.

Appendix A. Supplementary data

Supplementary data to this article can be found online at https://doi.org/10.1016/j.jinorgbio.2025.112875.

Data avalability

The data supporting this article have been included as part of the Supplementary Information.

References

[1] L. Li, P.K. Moore, An overview of the biological significance of endogenous gases: new roles for old molecules, Biochem. Soc. Trans. 35 (2007) 1138–1141, https://doi.org/10.1042/BST0351138.
[2] L. Li, P.K. Moore, Putative biological roles of hydrogen sulfide in health and disease: a breath of not so fresh air? Trends Pharmacol. Sci. 29 (2008) 84–90, https://doi.org/10.1016/j.tips.2007.11.003.
[3] H. Kimura, Signaling molecules: hydrogen sulfide and polysulfide, Antioxid. Redox Signal. 22 (2014) 362–376, https://doi.org/10.1089/ars.2014.5869.
[4] H. Kimura, Signaling by hydrogen sulfide (H_2S) and Polysulfides (H_2S_n) and the interaction with other signaling pathways, Hydrogen Sulfide (2022) 27–47, https://doi.org/10.1002/9781119799900.ch2.
[5] S.B. Singh, H.C. Lin, Hydrogen sulfide in physiology and diseases of the digestive tract, Microorganisms 3 (2015) 866–889, https://doi.org/10.3390/microorganisms3040866.
[6] M. Whiteman, S. Le-Trionnaire, M. Chopra, B. Fox, J. Whatmore, Emerging role of hydrogen sulfide in health and disease: critical appraisal of biomarkers and pharmacological tools, Clin. Sci. 121 (2011) 459–488, https://doi.org/10.1042/CS20110267.
[7] K.G. Fosnacht, M.D. Pluth, Activity-based fluorescent probes for hydrogen sulfide and related reactive sulfur species, Chem. Rev. 124 (2024) 4124–4257, https://doi.org/10.1021/acs.chemrev.3c00683.
[8] M. Strianese, M. Lamberti, C. Pellecchia, Interaction of monohydrogensulfide with a family of fluorescent pyridoxal-based Zn(ii) receptors, Dalton Trans. 47 (2018) 17392–17400, https://doi.org/10.1039/c8dt03969k.
[9] M. Strianese, M. Lamberti, A. Persico, C. Pellecchia, Reactivity of monohydrogensulfide with a suite of pyridoxal-based complexes: a combined NMR, ESI-MS, UV-visible and fluorescence study, Inorg. Chim. Acta 501 (2019) 119235–119241, https://doi.org/10.1016/j.ica.2019.119235.
[10] M. Strianese, C. Pellecchia, Fluorescent probes for H_2S detection: metal-based approaches, Hydrogen Sulfide (2022) 203–233, https://doi.org/10.1002/9781119799900.ch9.
[11] M. Strianese, G. Ferrara, V. Vykhovanets, N. Blal, D. Guarnieri, A. Landi, M. Lamberti, A. Peluso, C. Pellecchia, Sol-gel dipping devices for H_2S visualization, Sensors 23 (2023) 2023–2037, https://doi.org/10.3390/s23042023.
[12] G. Zauner, M. Strianese, L. Bubacco, T.J. Aartsma, A.W.J.W. Tepper, G.W. Canters, Type-3 copper proteins as biocompatible and reusable oxygen sensors, Inorg. Chim. Acta 361 (2008) 1116–1121, https://doi.org/10.1016/j.ica.2007.08.018.
[13] M.D. Hartle, M. Delgado, J.D. Gilbertson, M.D. Pluth, Stabilization of a Zn(ii) hydrosulfido complex utilizing a hydrogen-bond accepting ligand, Chem. Commun. 52 (2016) 7680–7682, https://doi.org/10.1039/C6CC01373B.
[14] M.D. Hartle, S.K. Sommer, S.R. Dietrich, M.D. Pluth, Chemically reversible reactions of hydrogen sulfide with metal phthalocyanines, Inorg. Chem. 53 (2014) 7800–7802, https://doi.org/10.1021/ic500664c.
[15] M.D. Hartle, M.R. Tillotson, J.S. Prell, M.D. Pluth, Spectroscopic investigation of the reaction of metallo-protoporphyrins with hydrogen sulfide, J. Inorg. Biochem. 173 (2017) 152–157, https://doi.org/10.1016/j.jinorgbio.2017.04.021.
[16] M.D. Pluth, Z.J. Tonzetich, Hydrosulfide complexes of the transition elements: diverse roles in bioinorganic, cluster, coordination, and organometallic chemistry, Chem. Soc. Rev. 49 (2020) 4070–4134, https://doi.org/10.1039/C9CS00570F.
[17] E. Galardon, A. Tomas, P. Roussel, I. Artaud, New fluorescent zinc complexes: towards specific sensors for hydrogen sulfide in solution, Dalton Trans. 42 (2009) 9126–9130, https://doi.org/10.1039/B907115F.
[18] E. Galardon, A. Tomas, M. Selkti, P. Roussel, I. Artaud, Synthesis, characterization, and reactivity of Alkyldisulfanido zinc complexes, Inorg. Chem. 48 (2009) 5921–5927, https://doi.org/10.1021/ic900238v.
[19] S. Milione, C. Capacchione, C. Cuomo, M. Strianese, V. Bertolasi, A. Grassi, New zinc complexes bearing k 2-Heteroscorpionate ligands: influence of second-sphere bonding interactions on reactivity and properties, Inorg. Chem. 48 (2009) 9510–9518, https://doi.org/10.1021/ic901091e.
[20] M. Dulac, A. Melet, E. Galardon, Reversible detection and quantification of hydrogen sulfide by fluorescence using the hemoglobin I from Lucina pectinata, ACS Sens. 3 (2018) 2138–2144, https://doi.org/10.1021/acssensors.8b00701.
[21] M. Strianese, D. Pappalardo, M. Mazzeo, M. Lamberti, C. Pellecchia, The contribution of metalloporphyrin complexes in molecular sensing and in sustainable polymerization processes: a new and unique perspective, Dalton Trans. 50 (2021) 7898–7916, https://doi.org/10.1039/d1dt00841b.
[22] M. Strianese, G.J. Palm, D. Kohlhause, L.A. Ndamba, L.C. Tabares, C. Pellecchia, Azurin and HS^-: towards implementation of a sensor for HS^- detection, Eur. J. Inorg. Chem. 2019 (2019) 885–891, https://doi.org/10.1002/ejic.201801399.
[23] M. Strianese, D. Guarnieri, M. Lamberti, A. Landi, A. Peluso, C. Pellecchia, Fluorescent salen-type Zn(II) complexes as probes for detecting hydrogen sulfide and its anion: bioimaging applications, Inorg. Chem. 59 (2020) 15977–15986, https://doi.org/10.1021/acs.inorgchem.0c02499.
[24] M. Strianese, G.J. D'Auria, M. Lamberti, A. Landi, A. Peluso, A. Varriale, S. D'Auria, C. Pellecchia, Salen, salan and salalen zinc(ii) complexes in the

interaction with HS^-: time-resolved fluorescence applications, Dalton Trans. 52 (2023) 1357–1365, https://doi.org/10.1039/D2DT03730K.
[25] J.R. Shapley, J.A. Osborn, Rapid intramolecular rearrangements in pentacoordinate transition metal compounds, Acc.Chem.Res. 6 (1973) 305–312, https://doi.org/10.1021/ar50069a004op.
[26] G. Consiglio, S. Failla, I.P. Oliveri, R. Purrello, S. Di Bella, Controlling the molecular aggregation. An amphiphilic Schiff-base zinc(II) complex as supramolecular fluorescent probe, Dalton Trans. 47 (2009) 10426–10428, https://doi.org/10.1039/B914930A.
[27] G. Consiglio, I.P. Oliveri, S. Failla, S. Di Bella, On the aggregation and sensing properties of zinc(II) Schiff-Base complexes of Salen-type ligands, Molecules 24 (2019) 2514–2535, https://doi.org/10.3390/molecules24132514.
[28] S. Di Bella, Lewis acidic zinc(ii) salen-type Schiff-base complexes: sensing properties and responsive nanostructures, Dalton Trans. 50 (2021) 6050–6063, https://doi.org/10.1039/D1DT00949D.
[29] F. Dumur, E. Contal, G. Wantz, D. Gigmes, Photoluminescence of zinc complexes: easily tunable optical properties by variation of the bridge between the Imido groups of Schiff Base ligands, Eur. J. Inorg. Chem. 2014 (2014) 4186–4198, https://doi.org/10.1002/ejic.201402422.
[30] A.C. Chamayou, S. Lüdeke, V. Brecht, T.B. Freedman, L.A. Nafie, C. Janiak, Chirality and diastereoselection of Δ/Λ-configured tetrahedral zinc complexes through Enantiopure Schiff Base complexes: combined vibrational circular dichroism, density functional theory, ^{1}H NMR, and X-ray structural studies, Inorg. Chem. 50 (2011) 11363–11374, https://doi.org/10.1021/ic2009557.
[31] C. Evans, D. Luneau, New Schiff base zinc(ii) complexes exhibiting second harmonic generation, J. Chem. Soc. Dalton Trans. 1 (2002) 83–86, https://doi.org/10.1039/B104360A.
[32] M. Enamullah, V. Vasylyeva, C. Janiak, Chirality and diastereoselection of Δ/Λ -configured tetrahedral zinc(II) complexes with enantiopure or racemic Schiff base ligands, Inorg. Chim. Acta 408 (2013) 109–119, https://doi.org/10.1016/j.ica.2013.08.016.
[33] T. Onodera, T. Akitsu, Tuning of the optical properties of chiral Schiff base Zn(II) complexes by substituents, Polyhedron 59 (2013) 107–114, https://doi.org/10.1016/j.poly.2013.04.051.
[34] L. Liu, X. Shang, R. He, J. Li, Y. Chen, H. Chen, T. Wang, Anion binding ability and cytotoxicity of a selective colorimetric chemosensor for H_2S based on Zn(II) complex, Inorg. Chim. Acta 495 (2019) 118994–119001, https://doi.org/10.1016/j.ica.2019.118994.
[35] D. Saren, E. Zangrando, H. Puschmann, S.C. Manna, Tridentate chelating ligand based fluorescent Zn(ii) coordination compounds for highly selective detection of picric acid, New J. Chem. 48 (2024) 4821–4830, https://doi.org/10.1039/D3NJ05089K.
[36] F. Santulli, G. Gravina, M. Lamberti, C. Tedesco, M. Mazzeo, Zinc and magnesium catalysts for the synthesis for PLA and its degradation: clues for catalyst design, Mol. Catal. 528 (2022) 112480–112488, https://doi.org/10.1016/j.mcat.2022.112480.
[37] S. D'Aniello, S. Laviéville, F. Santulli, M. Simon, M. Sellitto, C. Tedesco, C. M. Thomas, M. Mazzeo, Homoleptic phenoxy-imine pyridine zinc complexes: efficient catalysts for solvent free synthesis and chemical degradation of polyesters, Catal. Sci. Technol. 12 (2022) 6142–6154, https://doi.org/10.1039/d2cy01092e.
[38] F. Santulli, D. Pappalardo, M. Lamberti, A. Amendola, C. Barba, A. Sessa, G. Tepedino, M. Mazzeo, Simple and efficient zinc catalysts for synthesis and chemical degradation of polyesters, ACS Sustain. Chem. Eng. 11 (2023) 15699–15709, https://doi.org/10.1021/acssuschemeng.3c04927.
[39] F. Santulli, M. Lamberti, M. Mazzeo, A single catalyst for promoting reverse processes: synthesis and chemical degradation of polylactide, ChemSusChem 14 (2021) 5470–5475, https://doi.org/10.1002/cssc.202101518.
[40] Joseph Lakowicz, Principles of Fluorescence Spectrscopy, Spinger, 2006, https://doi.org/10.1007/978-0-387-46312-4.
[41] L.A. Currie, Detection and quantification limits: origins and historical overview, Anal. Chim. Acta 391 (1999) 127–134, https://doi.org/10.1016/S0003-2670(99)00105-1.
[42] Analytical Methods Committee, Recommendations for the definition, estimation and use of the detection limit, Analyst 112 (1987) 199–204, https://doi.org/10.1039/AN9871200199.
[43] M.Y. Guo, X.J. Liu, X. Zhang, Y.S. Yang, W.X. Sun, C. Xu, H.L. Zhu, A cytoplasm-applicative aggregation-induced fluorescent probe for detecting hydrogen sulfide and imaging study, Dyes Pigments 230 (2024) 112284–112291, https://doi.org/10.1016/j.dyepig.2024.112284.
[44] R. Sanokawa-Akakura, E.A. Ostrakhovitch, S. Akakura, S. Goodwin, S. Tabibzadeh, A H_2S-Nampt dependent energetic circuit is critical to survival and cytoprotection from damage in cancer cells, PLoS One 9 (2014) e108537, https://doi.org/10.1371/journal.pone.0108537.
[45] Y. Zhao, D.G. Truhlar, The M06 suite of density functionals for main group thermochemistry, thermochemical kinetics, noncovalent interactions, excited states, and transition elements: two new functionals and systematic testing of four M06-class functionals and 12 other functionals, Theor. Chem. Account 120 (2008) 215–241, https://doi.org/10.1007/s00214-007-0310-x.
[46] F. Weigend, Accurate coulomb-fitting basis sets for H to Rn, Phys. Chem. Chem. Phys. 8 (2006) 1057–1061, https://doi.org/10.1039/B515623H.
[47] F. Weigend, R. Ahlrichs, Balanced basis sets of split valence, triple zeta valence and quadruple zeta valence quality for H to Rn: design and assessment of accuracy, Phys. Chem. Chem. Phys. 7 (2005) 3297–3305, https://doi.org/10.1039/B508541A.
[48] A.V. Marenich, C.J. Cramer, D.G. Truhlar, Universal solvation model based on solute Electron density and on a continuum model of the solvent defined by the bulk dielectric constant and atomic surface tensions, J. Phys. Chem. B 113 (2009) 6378–6396, https://doi.org/10.1021/jp810292n.
[49] M. Rombach, H. Vahrenkamp, Pyrazolylborate-zinc-hydrosulfide complexes and their reactions, Inorg. Chem. 40 (2001) 6144–6150, https://doi.org/10.1021/ic010510+.
[50] J. Aron, C. Nicholas, Dynamic correlation, Mol. Phys. 99 (2001) 607–615, https://doi.org/10.1080/00268970010023435.
[51] S. Grimme, Supramolecular binding thermodynamics by dispersion-corrected density functional theory, Chem. Eur. J. 18 (2012) 9955–9964, https://doi.org/10.1002/chem.201200497.
[52] G. Luchini, J.V. Egre-Requena, I. Funes-Ardoiz, R.S. Paton, GoodVibes: Automated Thermochemistry for Heterogeneous Computational Chemistry Data, F1000Research 9, 2020, pp. 291–300, https://doi.org/10.12688/f1000research.22758.1.
[53] C. Riplinger, P. Pinski, U. Becker, E.F. Valeev, F. Neese, Sparse maps-a systematic infrastructure for reduced-scaling electronic structure methods. II. Linear scaling domain based pair natural orbital coupled cluster theory, J. Chem. Phys. 144 (2016) 024109, https://doi.org/10.1063/1.4939030.
[54] R.A. Kendall, T.H. Dunning, R.J. Harrison, Electron affinities of the first-row atoms revisited. Systematic basis sets and wave functions, J. Chem. Phys. 96 (1992) 6796–6806, https://doi.org/10.1063/1.462569.
[55] M. Garcia-Ratés, F. Neese, Effect of the solute cavity on the solvation energy and its derivatives within the framework of the Gaussian charge scheme, J. Comput. Chem. 41 (2019) 922–939, https://doi.org/10.1002/jcc.26139.
[56] F. Neese, The ORCA program system, WIREs Comput. Mol. Sci. 2 (2011) 73–78, https://doi.org/10.1002/wcms.81.
[57] M.J. Frisch, G.W. Trucks, H.B. Schlegel, G.E. Scuseria, M.A. Robb, J.R. Cheeseman, G. Scalmani, V. Barone, G.A. Petersson, H. Nakatsuji, X. Li, M. Caricato, A. V. Marenich, J. Bloino, B.G. Janesko, R. Gomperts, B. Mennucci, H.P. Hratchian, J. V. Ortiz, A.F. Izmaylov, J.L. Sonnenberg, Ding F. Williams, F. Lipparini, F. Egidi, J. Goings, B. Peng, A. Petrone, T. Henderson, D. Ranasinghe, V.G. Zakrzewski, J. Gao, N. Rega, G. Zheng, W. Liang, M. Hada, M. Ehara, K. Toyota, R. Fukuda, J. Hasegawa, M. Ishida, T. Nakajima, Y. Honda, O. Kitao, H. Nakai, T. Vreven, K. Throssell, J.E. Montgomery Jr Peralta, F. Ogliaro, M.J. Bearpark, J.J. Heyd, E. N. Brothers, K.N. Kudin, V.N. Staroverov, T.A. Keith, R. Kobayashi, J. Normand, K. Raghavachari, A.P. Rendell, J.C. Burant, S.S. Iyengar, J. Tomasi, M. Cossi, J. M. Millam, M. Klene, C. Adamo, R. Cammi, J.W. Ochterski, R.L. Martin, K. Morokuma, O. Farkas, J.B. Foresman, D.J. Fox, Gaussian 16 Rev. B01, Ref Type: Computer Program, Wallingford, CT, 2016.
[58] G. Schaftenaar, J.H. Noordik, Molden: a pre- and post-processing program for molecular and electronic structures, J. Comput. Aided Mol. Des. 14 (2000) 123–134, https://doi.org/10.1023/a:1008193805436.
[59] Dennington Roy, Todd A. Keith, Millam M. John, GaussView, Version 6.1, Semichem Inc., Shawnee Mission, KS, 2016 (Ref Type: Computer Program).
[60] M. Lamberti, M.V. Galotto, E. Vasca, A. Landi, A. Peluso, M. Strianese, Effect of metal coordination environment on the stability of zinc complexes and their reactivity with NaSH, ChemistrySelect 9 (2024) e202401334, https://doi.org/10.1002/slct.202401334.
[61] M. Strianese, V. Vykhovanets, N. Blal, D. Guarnieri, A. Landi, M. Lamberti, A. Peluso, C. Pellecchia, Paper-strip-based sensors for H_2S detection: a proof-of-principle study, Sensors 22 (2022) 3173–3186, https://doi.org/10.3390/s22093173.
[62] A.W. Kleij, M. Kuil, D.M. Tooke, A.L. Spek, J.N.H. Reek, Metal-directed self-assembly of a ZnII-salpyr complex into a supramolecular vase structure, Inorg. Chem. 46 (2007) 5829–5831, https://doi.org/10.1021/ic700408v.
[63] A.W. Kleij, M. Kuil, D.M. Tooke, M. Lutz, A.L. Spek, J.N.H. Reek, ZnII-Salphen complexes as versatile building blocks for the construction of supramolecular box assemblies, Chem. Eur. J. 11 (2005) 4743–4750, https://doi.org/10.1002/chem.200500227.
[64] A.W. Kleij, Zinc-centred salen complexes: versatile and accessible supramolecular building motifs, Dalton Trans. 24 (2009) 4635–4639, https://doi.org/10.1039/b902866h.
[65] A.W. Kleij, M. Kuil, M. Lutz, D.M. Tooke, A.L. Spek, P. Kamer, P.W.N.M. van Leeuwen, J.N.H. Reek, Supramolecular zinc(II)salphen motifs: reversible dimerization and templated dimeric structures, Inorg. Chim. Acta 359 (2006) 1807–1814, https://doi.org/10.1016/j.ica.2005.06.069.
[66] E.C. Escudero-Adân, J. Et-Buchholz, A.W. Kleij, Supramolecular adsorption of alkaloids by metallosalphen complexes, Inorg.Chem. 47 (2008) 4256–4263, https://doi.org/10.1021/ic702257e.
[67] M.E. Germain, T.R. Vargo, P.G. Khalifah, M.J. Knapp, Fluorescent detection of Nitroaromatics and 2,3-dimethyl- 2,3-dinitrobutane (DMNB) by a zinc complex: (salophen)Zn, Inorg. Chem. 46 (2007) 4422–4429, https://doi.org/10.1021/ic062012c.
[68] J.A. Connor, M. Charlton, D.C. Cupertino, A. Lienke, M. McPartlin, I.J. Scowen, P. A. Tasker, Zinc(II) complexes of putative obligate tetrahedrally co-ordinating pro-ligands, J. Chem. Soc. Dalton Trans. 13 (1996) 2835–2838, https://doi.org/10.1039/DT9960002835.
[69] A. La Cort, L. Mandolini, C. Pasquini, K. Rissanen, L. Russo, L. Schiaffino, Zinc-salophen complexes as selective receptors for tertiary amines, New J. Chem. 31 (2007) 1633–1638, https://doi.org/10.1039/B700723J.
[70] H.C. Lin, C.C. Huang, C.H. Shi, Y.H. Liao, C.C. Chen, Y.C. Lin, Y.H. Liu, Synthesis of alkynylated photo-luminescent Zn(ii) and Mg(ii) Schiff base complexes, Dalton Trans. 7 (2007) 781–791, https://doi.org/10.1039/B615380A.
[71] R.R. Holmes, Structure of cyclic pentacoordinated molecules of main group elements, Acc. Chem. Res. 12 (1979) 257–265, https://doi.org/10.1021/ar50139a006.

[72] R.S. Berry, Correlation of rates of intramolecular tunneling processes, with application to some group V compounds, J. Chem. Phys. 32 (1960) 933–938, https://doi.org/10.1063/1.1730820.
[73] R.J. Gillespie, 895. The stereochemistry of five-co-ordination. Part I. Non-transition elements, J. Chem. Soc. (1963) 4672–4678, https://doi.org/10.1039/JR9630004672.
[74] R.R. Holmes, Spectroscopy and structure of pentacoordinated molecules, Acc. Chem. Res. 5 (1972) 296–303, https://doi.org/10.1021/ar50057a002.
[75] A.W. Addison, T.N. Rao, J. Reedijk, J. van Rijn, G.C. Verschoor, Synthesis, structure, and spectroscopic properties of copper(II) compounds containing nitrogen-Sulphur donor ligands; the crystal and molecular structure of aqua[1,7-bis (N-methylbenzimidazol-2′-yl)-2,6-dithiaheptane]copper(II) perchlorate, J. Chem. Soc. Dalton Trans. 7 (1984) 1349–1356, https://doi.org/10.1039/DT9840001349.
[76] Z.Q. Liu, Y.M. Ng, P.J. Tiong, R.A. Bu Talip, N. Jasin, V.Y.M. Jong, M.G. Tay, Five-coordinate zinc(II) complex: synthesis, characterization, molecular structure, and antibacterial activities of bis-[(E)-2-hydroxy-N'-{1-(4-methoxyphenyl)ethylidene} benzohydrazido]dimethylsulfoxidezinc(II) Complex, Intl. J. Inorg. Chem. 2017 (2017) 7520640–7520648, https://doi.org/10.1155/2017/7520640.
[77] A. Gusev, V. Shul'gin, E. Braga, E. Zamnius, M. Kryukova, W. Linert, Luminescent properties of Zn complexes based on tetradentate N_2O_2-donor pyrazolone schiff bases, Dyes Pigments 183 (2020) 108626–108633, https://doi.org/10.1016/j.dyepig.2020.108626.
[78] M.A. El-Sayed, Triplet state. Its radiative and nonradiative properties, Acc.Chem. Res. 1 (1968) 8–16, https://doi.org/10.1021/ar50001a002.
[79] M. Schrader, R. Wodopia, H. Fahimi, Induction of tubular peroxisomes by UV irradiation and reactive oxygen species in HepG2 cells, J. Histochem. Cytochem. 47 (1999) 1141–1148, https://doi.org/10.1177/002215549904700906.
[80] X. Jiang, M.R. MacArthur, J.H. Treviño-Villarreal, P. Kip, C.K. Ozaki, S.J. Mitchell, J.R. Mitchell, Intracellular H_2S production is an autophagy-dependent adaptive response to DNA damage, Cell Chem. Biol. 28 (2021) 1669–1678, https://doi.org/10.1016/j.chembiol.2021.05.016.
[81] R.P. Rastogi, A. Richa, M.B. Kumar, R.P.Sinha Tyagi, Molecular mechanisms of ultraviolet radiation-induced DNA damage and repair, J. Nucleic Acids 2010 (2010) 592980–593012, https://doi.org/10.4061/2010/592980.